# Quantum Well Carrier Sweep Out: Relation to Electroabsorption and Exciton Saturation

A. Mark Fox, David A. B. Miller, *Senior Member, IEEE*, Gabriela Livescu, J. E. Cunningham, and William Y. Jan

*Abstract*—**We have studied the effects of changing the barrier design of GaAs–$Al_xGa_{1-x}As$ quantum wells on the electroabsorption, exciton saturation, and carrier sweep-out times. Five samples have been studied with $x$ values ranging from 0.2 to 0.4, and barrier thicknesses from 35 to 95 Å. Within this range, we find that the electroabsorption is not very sensitive to the barrier thickness, but that the ionization field of the excitons approximately doubles for an increase of $x$ from 0.2 to 0.4. The samples with high, thick barriers have lower internal quantum efficiencies than those with low, thin barriers. We find that the exciton saturation intensity increases with increasing applied field, and decreasing barrier thickness or height. These findings are adequately explained by the field and barrier dependence of the thermionic emission and tunneling sweep-out rates. Time-resolved electroabsorption measurements confirm our understanding of the variation in sweep-out rates between samples, and indicate that the escape mechanism at low field is probably a thermally-assisted tunneling process.**

## I. Introduction

THE physical mechanisms by which carriers escape from quantum wells under the influence of electric fields are an important factor in determining the performance of quantum well electroabsorptive devices such as the self-electrooptic effect device (SEED) [1], [2]. These are devices which operate by the quantum confined Stark effect, in which the excitons red-shift and broaden when an electric field is applied perpendicular to the quantum well layers [3]. If the carriers are swept out of the wells too rapidly on increasing the field, the broadening can increase. From this point of view, it is desirable to have quantum wells with relatively long sweep-out times, so that the excitons are sharper and can persist up to higher field levels. On the other hand, other physical properties of the quantum wells are favored by short sweep-out times. For example, there may be applications which require very fast switching times from single devices, and this would clearly be favored by having a faster sweep-out rate. Boyd *et al.* have recently demonstrated that the switching time of symmetric SEED devices can be made as short as 33 ps by using appropriately designed quantum wells with very fast carrier sweep-out times [4]. Another important property which is affected by the sweep out is the exciton saturation intensity. This, in fact, turns out to be an extremely important consideration in the design of SEED systems, because these systems tend to run at intensity levels much greater than that required to switch a single device. The reason for this is the need to pass on sufficient energy to the next device in the system to switch it after allowing for losses between consecutive devices. At these high power levels, the exciton absorption saturates, and this puts an effective upper limit on the maximum intensity which can be used. The system speed is determined by the time to integrate sufficient energy to switch the state of the devices, and therefore exciton saturation effects become the limiting factor in determining the maximum bit rate [5]. In a recent publication we have shown how the saturation intensity is strongly affected by the design of the quantum well structure, and that this effect is most likely caused by the change in carrier sweep-out times which accompanied the change in design [6].

In this paper we consider the physical processes which affect the carrier sweep-out rate in quantum wells subject to a perpendicular electric field, and we discuss how the sweep-out time is related to the electroabsorption and the exciton saturation intensity. We present a series of results on five carefully designed GaAs–AlGaAs quantum well structures which have allowed us to understand better the key physical mechanisms of thermionic emission and tunneling. We have thus been able to measure the dependence of the electroabsorption and exciton saturation intensity as a function of barrier design, electric field, and temperature. We have also measured the sweep-out times directly for two of the samples. From these measurements we have been able to come to a fairly clear understanding of the main trends in the sweep-out rate, and our conclusions have general applicability to other quantum well material systems, provided due consideration is given to the important material-dependent parameters. The paper is organized as follows. In Section II we discuss the basic physics that determines the sweep-out rate. In Section III we give details of the samples studied. In Sections IV and V we describe, respectively, the electroabsorption performance and exciton saturation intensity measured for the five samples. In Section VI we describe our direct measurements for the field and temperature dependence of the sweep-out times for two of the samples, and compare it to a third reference sample. In Section VII we gather together the various results and come to our conclusions.

Manuscript received December 7, 1990; revised April 30, 1991.

A. M. Fox is with AT&T Bell Laboratories, Holmdel, NJ 07733, on leave from the Clarendon Laboratory, Oxford OX1 3PU, England.

D. A. B. Miller, J. E. Cunningham, and W. Y. Jan are with AT&T Bell Laboratories, Holmdel, NJ 07733.

G. Livescu is with the Solid-State Technology Center, AT&T Bell Laboratories, Breinigsville, PA 18031.

IEEE Log Number 9101810.

## II. Carrier Sweep-Out Mechanisms

There are three physical mechanisms that contribute to the field dependence of the carrier lifetime $\tau$ in a quantum well in an electric field: recombination, thermionic emission, and tunneling. In Fig. 1 we give a schematic diagram that illustrates these three processes. On the assumption that the three mechanisms are independent of each other, we may write:

$$\frac{1}{\tau} = \frac{1}{\tau_R} + \frac{1}{\tau_E} + \frac{1}{\tau_T} \tag{1}$$

where $\tau_R^{-1}$, $\tau_E^{-1}$, and $\tau_T^{-1}$ are the recombination, thermionic emission, and tunneling rates, respectively. As will become clearer, $\tau$ is determined by a number of key parameters. These include: intrinsic material properties such as the carrier effective masses and band discontinuities; sample dependent factors such as the quantum well and barrier thickness; and external factors, such as the temperature and field strength. The three different mechanisms respond differently to changes in the various parameters, and so we shall consider each separately.

We consider first the carrier recombination rate. This is not in fact a sweep-out mechanism at all, and therefore does not contibute to the current measured in a photocurrent measurement. In good samples, the recombination rate is basically determined by the radiative lifetime, which is closely related to the electron-hole overlap and the occupancy factors [7]:

$$\frac{1}{\tau_B} \propto \sum_{n,n'} \left[ |\langle \phi_{en} | \phi_{hn'} \rangle|^2 \int g_{\text{red}}(E) f_c (1 - f_v) E \, dE \right] \tag{2}$$

where $\tau_B$ is the bimolecular recombination lifetime. The summation is over all electron and hole sublevels in the quantum well. $\langle \phi_{en} | \phi_{hn'} \rangle$ is the electron-hole overlap (the interband matrix element is assumed to be independent of energy), $g_{\text{red}}$ is the reduced density of states, and $f_c$, $f_v$ are the conduction and valence band occupancies. The main functional dependence of $\tau_B$ is with respect to the temperature and the field strength. With increasing temperature, the radiative lifetime increases on account of the thermal spread of the carriers in the bands [8], while with increasing field the electron-hole overlap diminishes resulting again in an increase in $\tau_B$ [9]–[11]. In samples of poorer purity, effects such as trapping become increasingly more dominant. In most of our samples, it appears that essentially all of the photocarriers are collected except at very low fields in the samples with high or thick barriers. This tells us that $\tau_R$ is usually negligible in comparison to the faster tunneling and thermionic emission rates.

The thermionic emission lifetime is determined principally by the height of the barrier over which the carriers must be emitted. Schneider and von Klitzing have derived the following expression for the thermionic emission lifetime in a quantum well [12]:

$$\frac{1}{(\tau_E)_i} = \left( \frac{k_B T}{2\pi m_i L_w^2} \right)^{1/2} \exp - \left[ \frac{H_i(F)}{k_B T} \right]. \tag{3}$$

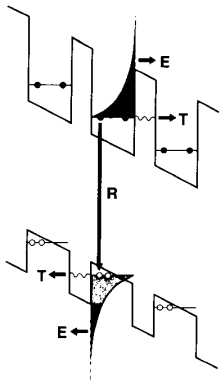


Fig. 1. Schematic band diagram of an optically excited quantum well in an electric field. The carrier loss mechanisms of recombination $R$, tunneling $T$, and thermal emission $E$ are indicated.

Here we have added a subscript $i$ to allow for the fact that the emission times of electrons and holes may differ ($i = e$ for electrons and $h$ for holes). In (3) $m_i$ is the effective mass in the quantum well, $L_w$ is the well width, $F$ is the electric field, and $T$ is the temperature. $H_i(F)$ is the field-dependent barrier height over which the carriers must be emitted. We have assumed that the emission rate against the field is negligible compared to that along the field, which will be true except at very low field strengths. Equation (3) was derived by assuming that the density of states close to the top of the barrier is essentially three dimensional, and that the carrier statistics are Boltzmann-like. The field dependence of the barrier height is simply given by

$$H_i(F) = Q_i \Delta E_g - E_i^{(n)} - |e| F L_w / 2 \tag{4}$$

where $Q_e / Q_h$ is the ratio of conduction to valence band discontinuities, ($Q_e + Q_h = 1$), $\Delta E_g$, is the difference in band gaps between the well and barrier material, and $E_i^{(n)}$ is the $n$th subband energy relative to the center of the well. Thus as the field is increased, the emission rate increases because the barrier height decreases. Note that the emission rate of electrons and holes is very different, and in the GaAs–AlGaAs system where $Q_e \approx 0.65$ [13], the holes can be emitted significantly *faster* than the electrons due to the smaller barrier height. Note also that the emission rate can be made faster by reducing $\Delta E_g$. This corresponds to using low values of $x$ in the GaAs–$Al_xGa_{1-x}As$ system.

The importance of thermionic emission for vertical transport in quantum wells has been widely studied in the context of CW transport and photocurrent measurements [14]–[16]. There is, however, very little information available about the dynamics of the thermionic emission process. It is not immediately clear whether the approach of Schneider and von Klitzing embodied in (3) is, in fact, appropriate for the SEED devices to which this paper is orientated. The reason is that (3) does not consider the time taken for the carriers to scatter from the subband in which they are excited optically to the quasi-continuum at the top of the well. In the case of SEED devices, the

photon energy is resonant with the $n = 1$ heavy hole exciton, which means that the carriers are created only in the first sublevel of the quantum wells. In order to be emitted, the thermalized carriers high up in the $n = 1$ sublevel must be scattered into the continuum states by carrier-carrier scattering or by interaction with phonons. If we assume that this scattering process is extremely efficient on account of the high density of states in the quasi-continuum, then (3) will be valid for the case of SEED devices.

The tunneling rate is determined by the quantum mechanical transmission of the particles through the finite potential barrier. Following the analysis of Larsson *et al.* [17], we write the tunneling rate from the $n$th sublevel as the product of the barrier collision frequency and the tunneling probability:

$$\frac{1}{(\tau_T)_i} = \frac{n\hbar\pi}{2L_w^2 m_i} \exp - \left[\frac{2L_b\sqrt{2m_{bi}H_i'(F)}}{\hbar}\right] \tag{5}$$

where $L_b$ is the barrier thickness and $m_{bi}$ is the effective mass in the barrier. In (5) we have taken the transmission of just a single barrier, which is the high field limit of the multiple barrier analysis of Larsson *et al.* Moreover, we have accounted for the variation in barrier height throughout the trapezoidal barrier in terms of an effective barrier height $H_i'$. As a first approximation, the tilted barriers can simply be averaged out, in which case $H_i'(F)$ would be the same as $H_i(F)$ in (4), only with $L_w$ replaced by $(L_w + L_b)$. A more sophisticated model would integrate over the varying potential throughout the barrier in an $\alpha$-decay type model [18]. We have used the simplified form in (5) to highlight the basic physical trends in the tunneling rate. The general charactersitics of the tunneling rate is that it increases with the field due to the reduction of the effective barrier height, and decreases with increasing barrier thickness. It is practically insensitive to the temperature, but depends strongly on the effective mass of the particle. This latter effect is the basis of "effective mass filtering" proposed by Capasso *et al.*, which uses the slower tunneling rate of the holes caused by their heavier effective mass [19].

The reduction in $\tau_T$ with increasing field was first studied in relation to the quenching of photoluminescence which occurs when the tunneling time becomes much less than the radiative recombination time [11], [20]–[23]. More recently, there have been a number of studies in which the tunneling time has been measured directly by way of resolving the photocurrent transients after short pulse excitation [24]–[26], or by time-resolved photoluminescence or nonlinear absorption optical spectroscopy [6], [18], [26]–[38]. These studies confirm that the tunneling rate does indeed decrease as the barrier thickness is increased, and is increased by an increase in the field strength. A particularly interesting phenomenon is that of resonant tunneling, where the field aligns sublevels in adjacent wells and the tunneling rate is enhanced by a coherent (or partially coherent) process. This enhancement of the tunneling rate at the resonant field has been directly observed by a number of groups [24]–[26], [32]–[34], [36]–[38]. From the point of view of devices, the enhanced tunneling rate is already potentially useful for sweeping the carriers out faster.

In writing (1) we made the approximation that the three carrier loss mechanisms contributing to the lifetime are independent of each other. This is not strictly true for thermionic emission and tunneling, because thermally assisted tunneling processes are possible. Larsson *et al.* proposed the thermal occupation of higher sublevels followed by rapid tunneling through the barrier as the escape mechanism for their GaAs–$Al_{0.25}Ga_{0.75}As$ quantum well p–i–n photodetectors [17]. Schneider *et al.* proposed a similar process to explain the temperature dependence of the photocurrent transients in a GaAs–AlAs superlattice [24]. Moreover, near the top of the barrier, the tunneling transmission may be so high that the effective barrier height for thermal emission is reduced (Fowler–Nordheim tunneling). Since it is both a tunneling and a thermal process, the probability for thermally assisted tunneling depends strongly on the barrier thickness as well as the barrier height and temperature. The expression for the escape probability by this process would contain a product of the exponentials on the right-hand side of (3) and (5) with the appropriate activation energy as $H_i(F)$ in (3) and with a reduced effective barrier height $H_i'(F)$ in (5).

On the basis of the discussion above, we can make some overall general observations about the sweep-out times. (We omit discussion of the recombination rate because, as discussed above, it is generally negligible for our samples.)

1) The sweep-out time decreases with increasing field because both the thermal emission and tunneling lifetimes decrease due to the reduction in the effective barrier height.

2) The sweep-out times increase with $L_b$ due to the increase in the tunneling time.

3) The sweep-out times increase with increasing $\Delta E_g$ due to the increase in both the thermal emission and tunneling times. For the GaAs–$Al_xGa_{1-x}As$ system, this implies that the sweep-out times increase with $x$.

4) The sweep-out times decrease with the temperature due to the decrease in the thermal emission time.

In trying to ascertain which of the sweep-out processes is dominant for a particular sample, it is useful to note that the hallmark of thermionic emission is its exponential dependence on $T^{-1}$, while tunneling is exponentially sensitive to the barrier thickness. Of course, a thermally-assisted tunneling process would be very sensitive both to temperature and barrier thickness.

In concluding this section it is worth emphasizing two points which are particularly relevant to the SEED and similar quantum well electroabsorptive devices. First, the sweep-out times of electrons and holes are very different due to their different effective masses and band discontinuities. This has a number of important implications for devices, especially as regards space charge effects [39]–[42]. Such space charge effects become increasingly more important at high power levels, especially in the

TABLE I
SAMPLE PARAMETERS FOR THE FIVE GaAs-$Al_xGa_{1-x}As$ p-i-n MULTIPLE QUANTUM WELL SAMPLES STUDIED. THE WELL WIDTH WAS 95 Å THROUGHOUT. ALL THE SAMPLES WERE DESIGNED TO HAVE A TOTAL QUANTUM WELL THICKNESS OF 1.0 $\mu$m. $L_b$ IS THE BARRIER THICKNESS. $\tau_E$ AND $\tau_T$ ARE THE CALCULATED THERMIONIC EMISSION AND SINGLE BARRIER TUNNELING TIMES FOR ELECTRONS AND HEAVY HOLES AT A FIELD STRENGTH OF $1.5 \times 10^4$ V $cm^{-1}$ AT ROOM TEMPERATURE

| Sample | $x$ | $L_b$ (Å) | Periods | $\tau_E$ (ps) (electrons) | $\tau_E$ (ps) (holes) | $\tau_T$ (ps) (electrons) | $\tau_T$ (ps) (holes) |
|---|---|---|---|---|---|---|---|
| I | 0.2 | 65 | 65 | 14 | 3.5 | 30 | $1.2 \times 10^4$ |
| II | 0.3 | 35 | 80 | 420 | 16 | 5.2 | 510 |
| III | 0.3 | 65 | 65 | 420 | 16 | 390 | $4.2 \times 10^5$ |
| IV | 0.3 | 95 | 55 | 420 | 16 | $2.7 \times 10^4$ | $3.1 \times 10^8$ |
| V | 0.4 | 65 | 65 | 9700 | 76 | 3300 | $1.1 \times 10^7$ |

$Ga_{0.47}In_{0.53}As$–InP system, which has a much larger valence band discontinuity than GaAs–$Al_{0.3}Ga_{0.7}As$. The hole sweep-out times are not always much slower than the electron times in the GaAs–AlGaAs system. This follows because of the smaller band discontinuity in the valence band which favors rapid thermal emission. It is also possible that valence band mixing effects can reduce the hole tunneling times compared to those of pure heavy hole states [43]. The second point is that SEED devices generally require about an optical absorption length of quantum well material, so that the devices contain a multiple quantum well structure rather than individual wells. Equations (1)–(5) are still valid for the sweep-out time from a particular well, but it is necessary to consider what happens to the carriers once they have escaped from the wells. The field strength is generally at least $10^4$ $Vcm^{-1}$, so that the carriers will be rapidly accelerated to the saturated drift velocity of $\sim 10^7$ $cms^{-1}$. Some of the carriers will be swept straight to the equipotentials in the contact layers, but others will be scattered and recaptured by subsequent wells. It is known that such capture events take place in less than 1 ps in InGaAs–InP quantum wells [44]. The net effect of recapture is to increase the effective sweep-out time.

## III. SAMPLE DESIGN

From the discussion in the previous section [points 1)–4)], it is clear that the sweep-out time depends critically on the electric field strength, the barrier thickness $L_b$ and barrier height (which is proportional to $x$). We therefore grew five p-i-n GaAs–$Al_xGa_{1-x}As$ multiple quantum well (MQW) samples by molecular beam epitaxy with the quantum wells as the intrinsic region of the diode. A controllable field could then be applied to the quantum wells by applying reverse bias to the diode. We designed the samples with the same well thickness (95 Å), but with varying barrier thickness $L_b$ and barrier Al concentration $x$. Table I gives details of the samples. Samples I, III, and V have the same barrier thickness (65 Å), but have the $x$ value varying from 0.2 to 0.4, while samples II, III, and IV have constant $x$ (0.3) but have $L_b$ varying from 35 to 95 Å. Note that we have varied the number of periods where necessary in samples II and IV, so that the total MQW thickness remains constant at 1.0 $\mu$m. This means that a given applied voltage corresponds to the same nominal field strength for all the samples. We regard sample III as a reference, since it has the same barrier design as many SEED devices.

The samples were grown on n-doped GaAs substrates. The detailed layer structure, starting from the substrate up, was as follows. 0.2 $\mu$m GaAs buffer layer ($n \sim 2 \times 10^{18}$ $cm^{-3}$), 1.2 $\mu$m $Al_{0.3}Ga_{0.7}As$ stop etch ($n \sim 5 \times 10^{17}$ $cm^{-3}$), 0.24 $\mu$m 15 Å/15 Å short period GaAs–$Al_xGa_{1-x}As$ superlattice ($n \sim 5 \times 10^{17}$ $cm^{-3}$), 1.0 $\mu$m intrinsic MQW structure (see Table I), 0.75 $\mu$m $Al_xGa_{1-x}As$ ($p \sim 5 \times 10^{17}$ $cm^{-3}$), 0.1 $\mu$m GaAs ($p^+ \sim 2 \times 10^{18}$ $cm^{-3}$). The samples were processed into 200 $\mu$m $\times$ 200 $\mu$m mesas, and after depositing gold contact pads on the top $p^+$ layer, the optical window was approximately 120 $\mu$m $\times$ 200 $\mu$m. For the room temperature electroabsorption measurements, tungsten probes were used to make contact to the samples, but wire bonding was required for the low temperature work. In the transmission measurements, the samples were mounted on sapphire or BK7 disks with clear epoxy, and the GaAs substrates were etched away using a jet etcher.

In the last four columns of Table I we indicate the values of $\tau_E$ and $\tau_T$ calculated for electrons and heavy holes at room temperature for our five samples from (3) and (5). We assumed a field strength of $1.5 \times 10^4$ $Vcm^{-1}$, which corresponds approximately to the built-in field of the diode at 0 V applied bias. As expected, the escape time for samples with low or thin barriers is lower than for those with high or thick barriers. It is clear that the dominant escape mechanism for the holes is thermal emission, while for electrons, the dominant mechanism depends on the details of the sample. Note how short the hole thermal emission times are. In particular, it is not generally true to presume that the hole escape rate is very much slower than the electron escape rate. This will depend on the sample design, the temperature, and the field strength.

## IV. ELECTROABSORPTION

In Fig. 2 we show representative photocurrent spectra for the five samples at room temperature. These spectra were taken using a tungsten lamp light source and 0.25 m monochromator with a resolution of $\sim 2$ meV. The voltages shown are the reverse bias applied to the diode. The

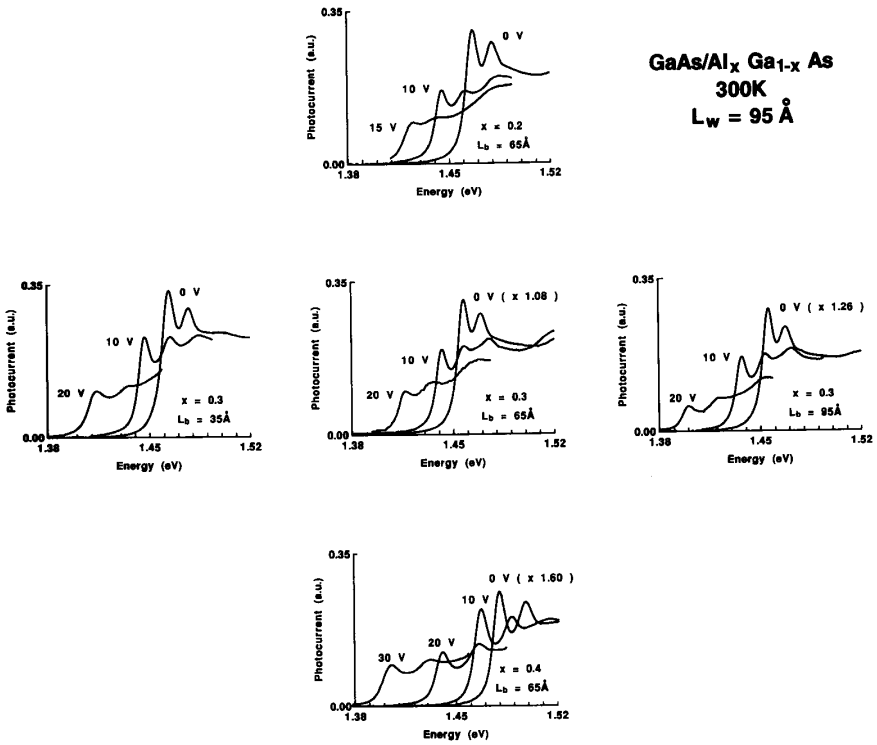


Fig. 2. Measured electroabsorption for our five samples at room temperature. The barrier thickness increases horizontally across the figure, while the barrier height increases vertically downwards.

five graphs are laid out so that $x$ varies vertically while $L_b$ varies across the figure. We notice immediately that all five samples show very good quantum confined Stark effect performance. Let us first consider the variation in electroabsorption with barrier thickness at constant $x$. For $x = 0.3$, we measure only small variations in the exciton linewidth and red-shift on varying $L_b$ from 95 to 35 Å. As discussed above, the principal effect of reducing the barrier thickness is to reduce the tunneling time. The reason why we do not see any large effect is that at room temperature, the linewidth is dominated by *LO*-phonon broadening and inhomogeneous broadening due to interface roughness and alloy disorder [45]. The thermal lifetime of the excitons is known to be only 300 fs at room temperature [46], which is much less than the 5 ps electron tunneling time calculated for the 35 Å barrier sample at 0 V (see Table I). However, there must ultimately come a point at which the thinness of the barrier does cause significant exciton line broadening, because the tunnelling time continues to decrease exponentially with the barrier thickness as the barrier is thinned further. In fact, we have also investigated samples grown with 25 and 15 Å $Al_{0.3}Ga_{0.7}As$ barriers. In these samples, the 0 V exciton linewidth *was* significantly larger than for samples II–IV, most noticeably for the 15 Å barrier sample, where the linewidth was broader by a factor ~1.3 at 5 V. From the point of view of devices, there appears to be no significant loss in electroabsorption involved in reducing the barrier thickness from 65 to 35 Å.

We now consider the variation of electroabsorption with the $x$ value of the barriers. On changing the $x$ value, we change the confinement energy of the carriers. This does appear to have a noticeable effect on the electroabsorption. For sample I with $x = 0.2$, the heavy hole exciton is barely resolved at 15 V, whereas for sample V with $x = 0.4$, the exciton is still well resolved at 30 V. The 80 meV exciton red-shift for sample V at 30 V bias (field $\sim 3 \times 10^5$ V cm$^{-1}$) is particularly noteworthy. This red-shift corresponds to about ten exciton binding energies. The results imply that the field for exciton ionization at least doubles on increasing $x$ from 0.2 to 0.4. The reason why the excitons are less stable to field in the samples with smaller $x$ is most likely that the carriers can be thermally emitted very rapidly over the relatively low barriers, which would give rise to lifetime broadening. Note that the electroabsorption of sample I with $x = 0.2$ is still very useable from the point of view of SEED devices. These devices require a large contrast between the low and high field absorption at the exciton wavelength, so that the main criterion is the 0 V exciton linewidth rather than the stability of the excitons to high fields. In fact, it is actually preferable that the excitons begin to broaden at more modest voltages, since then the voltage required for a particular contrast ratio decreases.

In order to get a meaningful comparison of the electroabsorption performance, we have scaled up the 0 V spectra for samples III–V by the factors shown in the figure. This was necessary because we took photocurrent rather than absorption spectra. The photocurrent $i$ generated for incident optical power $P$ is given by

$$i = P\frac{\eta(1-R)|e|}{\hbar\omega}[1-\exp(-\alpha L)]. \qquad (6)$$

Here, $\alpha$ is the absorption coefficient at the incident photon energy of $\hbar\omega$, $R$ is the reflectivity of the front surface, and $L$ is the total thickness of quantum well material. $\eta$ is the internal quantum efficiency of the photodiode; that is, the number of electrons collected per absorbed photon. The principal reason why $\eta$ would be different from unity is that the sweep-out time is comparable to the recombination time, in which case, a significant number of photoelectrons are lost from the current through recombination. The photocurrent spectra have the same general shape as the absorption spectra, with peaks at the same wavelength, but on making comparisons at different voltages, it is necessary to consider whether $\eta$ is unchanged with voltage. At 0 V we observed that the whole spectrum for samples III–V was scaled down compared to the spectrum at 5 V. This was not true for samples I and II, where, for example, we observed a monotonic decrease in the peak photocurrent at the heavy hole exciton as a function of voltage. By contrast, the heavy hole exciton photocurrent peak for samples III–V increased at first as the voltage was applied, reaching a maximum between 2.5 and 5.0 V, and thereafter decreased with voltage. The reason for this behavior is that $\eta$ is less than unity for samples III–V at low voltages because of their long sweep-out time. As the voltage is increased, $\eta$ increases to unity because the sweep-out time decreases compared to the recombination time. The scale-up factors in Fig. 2 were included to compensate for the nonunity $\eta$. In samples I and II, we observed that the photocurrent in the continuum states immediately above the heavy hole exciton was practically independent of voltage up to 5 V. We chose the scale-up values by comparing the magnitude of the photocurrent for samples III–V in the same spectral region at 0 and 5 V, i.e., we assume that only $\eta$ in (6) changes between 0 and 5 V at this photon energy. Thus the reciprocal of the scale-up factor gives an approximate measure of $\eta$ for the particular sample at 0 V. Note that this suggests that $\eta$ decreases with barrier thickness and with $x$, which is entirely consistent with points 2) and 3) in Section II.

We were able to verify directly that $\eta$ is indeed unity to within experimental error for sample I. This was done by measuring the photocurrent $I$–$V$ characteristic of the diode at low temperatures using a Hewlett Packard HP4145B semiconductor parameter analyzer, when the diode was illuminated with a known amount of laser power. Fig. 3 shows a schematic of the apparatus used. (The acoustooptic modulator was superfluous for this measurement, but was needed later for the saturation measurements.) For this measurement, the sample was mounted in a continuous flow Helium cryostat. Fig. 4 shows representative $I$–$V$ characteristics at 30 K for two different wavelengths at an incident power level of 3.8 $\mu$W. Consider first the $I$–$V$ for 807 nm excitation (dotted line). The laser wavelength is longer than the exciton line at 0 V, and as the voltage is increased, first the heavy hole exciton and then the light hole exciton is swept through the laser wavelength. Consider now the $I$–$V$ for 796 nm excitation (solid line). This wavelength is closer to the exciton at 0 V, and so the voltage required to bring the heavy hole exciton into resonance with the laser is smaller (2 V). As for 807 nm excitation, we see peaks corresponding to both the heavy and light hole excitons. There is a third peak, which we assign to resonant tunneling effects. Low temperature photocurrent spectra of this sample reveal an anomalous line broadening around 5 V corresponding to the resonant tunneling of electrons from the first sublevel in one well to the second sublevel in the adjacent well [47]. Returning to the heavy hole peak at $\sim$2 V, we notice that this heavy hole peak appears flattened. The reason for the flattened peak is that at these low temperatures and voltages, the exciton lines are very narrow, with a larger peak absorption height compared to room temperature. The absorbance $[1-\exp(-\alpha L)]$ is insensitive to $\alpha$ when $\alpha$ becomes very large, and so we see that the photocurrent becomes independent of voltage near the heavy hole peak. We can thus take $[1-\exp$

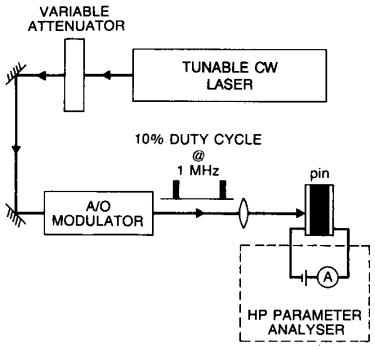


Fig. 3. Experimental apparatus for the quantum efficiency measurements and exciton saturation intensity measurements.

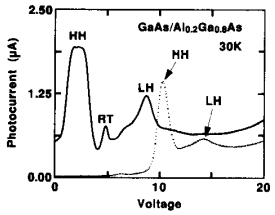


Fig. 4. Photocurrent $I$–$V$ spectrum for sample I at 30 K for excitation wavelengths of 796 nm (solid line) and 807 nm (dotted line). The incident power was 3.8 $\mu$W. The heavy hole (HH), light hole (LH), and resonant tunneling (RT) peaks are labelled.

$(-\alpha L)]$ equal to unity at the flattened peak, and thereby obtain a value of $\eta$ from (6), given that $P$ is known, and $(1 - R) \approx 0.7$ for GaAs. In this way we arrive at a value of unity for $\eta$ at 30 K and 2 V to within the estimated 20% absolute accuracy of the power meter. We were able to repeat this procedure up to 200 K, and found no significant departure of $\eta$ from unity in this temperature range. Above 200 K, the exciton peaks in the $I$–$V$ characteristics were rounded at all voltages, so that we could not deduce $\eta$ because $[1 - \exp(-\alpha L)]$ was not known. Throughout this paper we have assumed that $\eta$ remains essentially unity at and slightly above room temperature, as has been observed previously [1], [3], and confirmed in recent quantum efficiency measurements in samples with similar designs to ours [48]. This assumption is consistent with the fact that the peak exciton photocurrent measured in the spectra for samples I and II was a monotonically decreasing function of voltage, as discussed above. On the basis of this assumption, we could measure the room temperature $I$–$V$ characteristic of any of the five samples for varying laser wavelength and convert it to an $\alpha$-$V$ characteristic. We thus could obtain the values of the exciton absorption coefficient at room temperature as a function of voltage. The values of $\alpha$ deduced by assuming unity $\eta$ are in good agreement with direct measurements in similar conditions [3]. Given the discussion above, this conversion is less reliable for samples III–V at low voltages, and we have to make an estimate of the actual value of $\eta$ based on the electroabsorption scale-up factor.

## V. Exciton Saturation

Exciton saturation measurements were made using the apparatus shown in Fig. 3. The excitation source was either a CW Styryl 9 dye laser or a titanium sapphire laser. We used an acoustooptic modulator to produce a train of square wave pulses of 100 ns duration at a repetition rate of 1 MHz. This low 10% duty cycle was necessary in order to reduce thermal effects in the sample. Spot radii on the sample ranged from 2–30 $\mu$m. The experiment consisted in measuring the $I$–$V$ photocurrent characteristic of the diodes as a function of incident laser power and wavelength with an HP4145B semiconductor parameter analyzer. Fig. 5 shows typical results for two different wavelengths in sample V at room temperature. (Sample V is the one that saturates most easily because of its high barriers.) We have divided the photocurrent by the laser power to obtain the responsivity of the quantum wells, considering them as a photodiode. In this figure, positive voltage corresponds to reverse bias on the diode. The laser spot was Gaussian with a measured $e^{-2}$ radius ($w$) of 4.5 $\mu$m. In Fig. 5(a), the laser wavelength is 840 nm, approximately 5 nm longer than the heavy hole exciton at 0 V. The responsivity shows peaks at the voltages where the applied field exactly red-shifts the excitons to the laser wavelength, because the absorption has a maximum at the exciton wavelengths. Thus in Fig. 5(a) we first see a peak at 6 V corresponding to the heavy hole exciton, and then

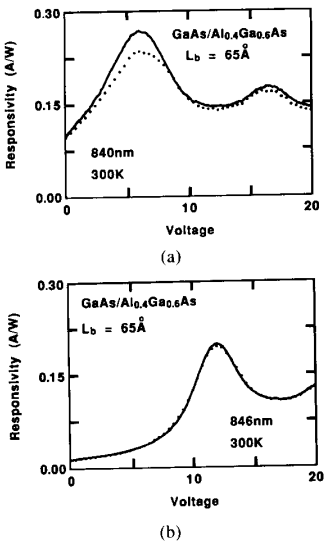


Fig. 5. Room temperature responsivity curves of sample V for two different wavelengths at incident power levels of either 0.4 $\mu$W (solid line) or 40 $\mu$W (dotted line).

at 16 V for the light hole exciton. The solid curve shows the responsivity measured at an incident power level of 0.4 $\mu$W, while the dotted curve shows the responsivity at 40 $\mu$W. The 40 $\mu$W curve follows the 0.4 $\mu$W curve fairly closely, except in the vicinity of the heavy hole peak. (The small down scaling of the 40 $\mu$W curve is probably just the experimental accuracy of our power measurements.) We measure less responsivity at the heavy hole peak at the higher power level, which we interpret as being caused by saturation of the excitons. In Fig. 5(b) we show the responsivities measured at the same power levels as for Fig. 5(a), but with the laser tuned to 846 nm. Now we must apply 12 V reverse bias to red-shift the heavy hole exciton to the laser wavelength, and the light hole is outside the range of the 20 V sweep. We observe negligible saturation at the heavy hole peak at the higher power level, which tells us that the saturation intensity has increased with the voltage. This is also why we do not observe any saturation at the light hole peak in Fig. 5(a).

In order to obtain a value for the heavy hole exciton saturation intensity at a particular voltage we proceed as follows. First we convert the responsivity at the heavy hole peak to an absorption coefficient using (6) with the assumption of $\eta = 1$. In Fig. 6 we show the values of $\alpha L$ deduced in this way as a function of average incident laser intensity $(P/\pi w^2)$. The data is for the heavy hole exciton at 6 V, as in Fig. 5(a). In the intensity range where the saturation varies linearly with intensity, the averaged intensity correctly accounts for the variation in the saturation across the spot size due to the Gaussian profile of the laser. If we assume a phenomenological absorption saturation dependence of the form

$$\alpha(I) = \frac{\alpha_0}{1 + (I/I_s)} \tag{7}$$

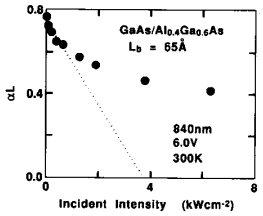


Fig. 6. Intensity dependence of the heavy hole exciton absorption in sample V at 6 V reverse bias.

then at low intensity $\alpha$ is a linear function of $I$, and $I_s$ is the extrapolated intercept on the intensity axis. We have shown the extrapolation of $\alpha(I)$ in Fig. 6, which gives an intercept at 3.7 kW cm$^{-2}$. In order to obtain the value of $I_s$ from the experimental data, we have to allow for the fact that the intensity $I$ in (5) is the *local* intensity inside the sample, while the data is measured against *incident* intensity. In the limit of small changes in $\alpha$, where the effective interaction length approximation is valid [45], $I_s$ can be obtained by multiplying the experimental intercept by $(1 - R)[1 - \exp(-\alpha_0 L)]/\alpha_0 L$. We thus obtain a value of 1.8 kW cm$^{-2}$ for the heavy hole exciton saturation intensity of sample V at 6 V and room temperature.

In Fig. 7 we show the 300 K saturation intensities of the heavy hole excitons as a function of reverse bias for the five samples. The values were obtained exactly as described in the previous paragraphs, with the same spot size throughout. The average field is determined by the applied voltage, the built-in voltage of the diode, and the intrinsic region width, and is therefore approximately the same for all the samples at a given voltage. From Fig. 7, we can draw three clear conclusions about $I_s$.

1) $I_s$ increases with applied field.
2) $I_s$ decreases with the barrier thickness $L_b$.
3) $I_s$ decreases with the barrier Al concentration $x$.

It is clear that thin barriers with low Al concentration give the best saturation performance for SEED's, and that careful design of the quantum well structure can lead to improved saturation performance.

We now discuss the physics behind the experimental behavior 1)–3). Exciton saturation in quantum wells has been extensively studied experimentally and theoretically in a variety of material systems for the case of zero electric field [45], [46], [49]–[58]. In the GaAs–AlGaAs system, for example, the heavy hole excitons are known to saturate at 300 K with a microscopic saturation areal density of $N_s$ of $\sim 3 \times 10^{11}$ cm$^{-2}$ for the case of zero applied field [45], [49]. The case of finite electric field has received less attention, with only a few studies published at present [6], [31], [42]. A quantitative analysis of $I_s$ at finite applied field is complicated by the fact that $\tau_e$ and $\tau_h$ are different, as discussed in Section II. Since the steady state areal carrier populations generated at a CW intensity $I$ are given by

$$N_i = \frac{I\alpha\tau_i(L_w + L_b)}{\hbar\omega} \tag{8}$$

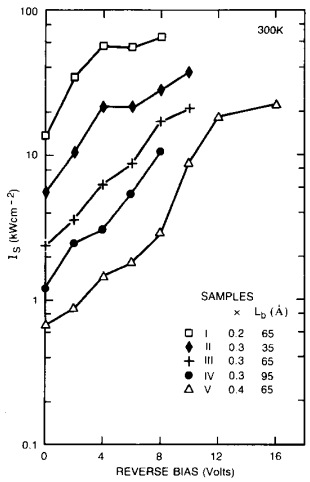


Fig. 7. Heavy hole exciton saturation intensity at room temperature as a function of applied reverse bias for the five GaAs–$Al_xGa_{1-x}As$ quantum well p-i-n samples.

we have therefore to consider the effect of having different electron and hole densities within the sample. There are two main consequences of this. First we must consider the different saturating efficiencies of the two particle types, and second, we have to consider the effects of space charge buildup. These two effects are discussed in more detail below. However, before going into details we can make some general observations which give the main ideas to explain the results. The principal point is that (8) shows that the carrier densities vary strongly with the sweep-out rate through $\tau_i$. This means that by reducing the sweep-out times we can reduce the carrier densities generated at a given intensity. Both space charge effects and microscopic exciton saturation depend on the carrier density, and thus by reducing the sweep-out time, we should be able to increase the exciton saturation intensity. The close parallel between 1)–3) *above* and points 1)–3) *in Section II*, confirms this supposition, and strongly suggests that the variation in $I_s$ between the samples is caused by differing tunneling and thermionic emission rates. This conclusion does not depend on the detailed microscopic mechanism of the exciton saturation.

The saturation of excitons by a gas of thermalized carriers, but with differing electron and hole populations, can be anlaysed by an extension of the methods of Schmitt-Rink *et al.* [57], [58]. At room temperature, where the carrier gases have Boltzmann distributions, the exciton saturation is essentially proportional to the number of carriers in the region of $k$ space up to $\sim 1/a_x$, where $a_x$ is the exciton radius. This implies that the saturation density for a *single* thermalized carrier type at high temperatures is proportional to its effective mass [see (2.3.37b) in [58]]. (The heavier carriers are distributed over a larger region of $k$ space.) The fractional exciton absorption saturation $\delta\alpha/\alpha_0$ is then given by

$$-\frac{\delta\alpha}{\alpha_0} = \frac{I}{I_s} = \frac{N_e}{N_{se}} + \frac{N_h}{N_{sh}}. \tag{9}$$

When $N_e = N_h = N$, the absorption saturation is simply $-\delta\alpha/\alpha_0 = N/N_s$. Therefore we deduce that the individual particle saturation densities $N_{si}$ are greater than $N_s$ by a factor $m_i/\mu$, where $\mu = m_e m_h/(m_e + m_h)$ is the reduced mass. Taking this into account, we can combine (8) and (9) to obtain

$$I_s = \frac{\hbar\omega N_s}{\alpha_0(L_w + L_b)} \frac{m_e + m_h}{m_e\tau_h + m_h\tau_e}. \tag{10}$$

In principle, (10) allows us to evaluate the exciton saturation intensity at finite applied field. In order to do this, we need detailed knowledge of the field dependence of both $\tau_e$ and $\tau_h$, and also of $N_s/\alpha_0$. $N_s/\alpha_0$ may change somewhat as the field is applied. $N_s$ is inversely proportional to $a_x^2$ [57], and $a_x$ has been calculated to increase by 25–40% on increasing the field from 0 to $10^5$ V cm$^{-1}$ in $\sim 100$ Å quantum wells [3], [59], [60]. This would cause a reduction in $N_s$ by a factor of $\sim 2$ at most. This decrease in $N_s$ is offset, to a large extent, by the accompanying decrease in $\alpha_0$. Therefore it is very unlikely that the field and barrier dependence of $N_s/\alpha_0$ can explain the experimental results. Therefore we expect the strong field and barrier dependence of $\tau_e$ and $\tau_h$ to dominate the field dependence of $I_s$.A quantitative analysis of (10) requires measurements of *both* $\tau_e$ and $\tau_h$ as a function of voltage, and this data is not yet available. However, our basic conclusion that the saturation intensity is dominated by the lifetimes is fully consistent with (10).

As mentioned above, the other consequence of having different electron and hole densities in the sample is the buildup of space charge as the intensity is increased. For example, if the electrons escape faster than the holes, then the holes are left behind and generate the space charge. The space charge can screen the applied field and generate field nonuniformities. The result is a reduction of the exciton red-shift produced by the external field, and also exciton broadening. Both these effects would change the absorption at the laser wavelength as the intensity is increased, and might therefore look like exciton saturation. Moreover, (3)–(5) shows that $\tau_e$ and $\tau_h$ can begin to depend on each other and on the laser intensity by means of the space charge modifications to the field. Steady-state space charge effects have been observed in InGaAs–InP [39]–[41], and Wood *et al.* have recently given a self-consistent analysis of the intensity dependent space-charge effects in this material [42]. These space charge effects are particularly acute in InGaAs–InP, where the hole sweep-out times are very slow because of the large band discontinuity for that system. It is reasonable to expect that steady state space charge effects in the GaAs–AlGaAs system will be less severe than in InGaAs–InP, because the band discontinuities are smaller, and the hole thermal emission times in GaAs–AlGaAs are expected to be fast (see Table I). We were able to see some evidence for space charge effects at low voltages in sample V, which has the largest band discontinuity of our five samples. Fig. 8 shows the responsivity of this sample with the laser tuned to 838 nm, such that the heavy hole exciton was red-shifted to the laser wavelength with 4 V reverse bias. As for Fig. 5, the solid and dotted lines are for 0.4 and 40 $\mu$W incident power. We notice that at the higher power level the heavy hole peak has saturated and shifted to about 5 V. This shift might well be caused by the buildup of space charge, since this effect would tend to reduce the field inside the sample, and thus we would have to apply more external voltage to bring the average internal field up to the level required to red-shift the exciton to the laser wavelength. (The shift cannot be explained in terms of series or contact resistance, because in that case the light hole exciton would also shift to higher voltages at the higher power level). Since the laser wavelength is fixed, and the exciton red-shift is determined by the magnitude of the internal field, we can be reasonably sure that the average internal field in the sample at 4 V and 0.4 $\mu$W power is the same as at 5 V and 40 $\mu$W power. Therefore, we can partly isolate the change in absorption due to space charge by following the exciton peak in the $I$–$V$ curve as the power is increased, rather than measuring the photocurrent at constant voltage. However, we could not completely eliminate space charge effects, because space-charge induced field nonuniformities cause exciton broadening, which leads to a reduction in the peak height even though the average field is unchanged. In practice, we found that the difference in $I_s$ between measuring the responsivity at fixed voltage as opposed to following the peak was about a factor 2, which is within the estimated absolute accuracy, and is much less than the variation between the samples and voltages.

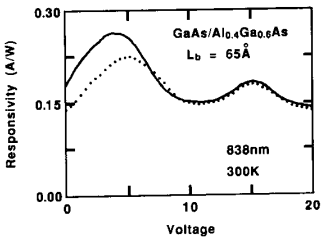


Fig. 8. Responsivity of sample V for 838 nm excitation at an incident power level of either 0.4 $\mu$W (solid line) or 40 $\mu$W (dotted line). The shift in the heavy hole peak to higher voltage with increasing power may be an indication of the importance of space charge effects in this sample at low voltages.

The highest saturation intensities were measured for sample I, which had $x = 0.2$ and $L_b = 65$ Å. Since this sample has the lowest barrier, and thermionic emission is more sensitive to the barrier height than tunneling [compare (3) and (5)], our understanding of this result is that the high saturation intensity is related to a very rapid thermal emission process. If this is indeed the case, then $I_s$ should be very sensitive to temperature. We therefore measured $I_s$ for this sample as a function of temperature. In Fig. 9, we plot $(I_s\alpha L\lambda T^{-1})$ against $T^{-1}$ between 60 and 360 K. The quantity $(I_s\alpha L\lambda T^{-1})$ was chosen based on (10) to highlight the temperature variation of $\tau_e$ and $\tau_h$ after

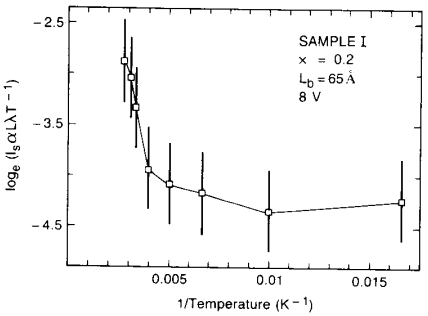


Fig. 9. Normalised temperature dependence of the heavy hole exciton saturation intensity for sample I at 8 V reverse bias.

allowing for the linear $T$ dependence of $N_s$ at high temperatures [57]. The applied voltage was 8 V. The measurement could not be made at lower voltage because the value of $[1 - \exp(-\alpha_0 L)]$ was too close to unity to give meaningful results from photocurrent measurements (see Fig. 4). We interpret the results as follows. $(I_s \alpha L \lambda T^{-1})$ is essentially independent of $T$ at low temperatures because the lifetimes are dominated by tunneling. As the temperature is raised, the thermal emission process becomes activated. The error bars on the measurements are unfortunately too large to obtain reliable values of the activation energy. The important result is the strong sensitivity to temperature, which confirms our intuition that the high saturation intensity measured at room temperature is caused by rapid thermal emission.

We close this section with a brief discussion of the estimated accuracy of our values of $I_s$. The Gaussian beam averaging and effective interaction length correction are accurate up to first order in $\delta\alpha/\alpha_0$. This is also true of the theoretical models used to write (9). We could not reliably detect values of $\delta\alpha/\alpha_0$ less than 2–3%, and our values of $I_s$ are based mainly on the intensities required to give $\delta\alpha/\alpha_0$ of ~5–10%. The first order approximation should be reasonable at these intensity levels. Also, at these relatively low power levels, our neglect of higher order many-body effects such as band-gap renormalization should be reasonable. Such effects become increasingly more important at higher intensities, and may be the reason why, for example, the data in Fig. 6 do not fit very accurately to the two-level saturable atom approximation of (7) at high intensity. We do not think that thermal effects are significant in our data. These would have shown up in the data such as Figs. 5 and 8 as a shift to *lower* voltage at high powers, which was never observed with the 10% high frequency duty cycle. We assumed that the internal quantum efficiency $\eta$ was unity and invariant with intensity. There is no reason to expect $\eta$ to vary with intensity in the limit of small $\delta\alpha/\alpha_0$. This follows because $\eta$ is determined by the ratio of the sweep-out time to the recombination time, and this should be unaffected by intensity to first order. The assumption of $\eta = 1$ affects the values of $\alpha L$ determined from the photocurrent spectra, but the values of $I_s$ deduced from extrapolating $\alpha(I)$ are not very sensitive to $\eta$ for the values of $\eta$ encountered in the samples (minimum value ~60%), provided $\eta$ is unchanged with intensity. Our absolute accuracy is affected by the accuracy of our value of the beam radius, and also the calibration of the power meter. A reasonable estimate for the absolute accuracy is a factor of 2. The principal result of our work is the variation of $I_s$ between the samples and with the applied voltage. This is a comparative study, with the measurements performed indentically for all the samples and voltages, and so the basic result is valid, irrespective of the validity of any of our approximations.

## VI. Carrier Sweep-Out Measurements

We made direct measurements of the sweep-out times of samples I and II by performing pump-probe experiments on transmission samples made from the same wafer as the previous measurements. A schematic diagram of the apparatus is given in Fig. 10. The samples were mounted in a continuous flow Helium cryostat for the temperature dependent measurements. The laser pulsewidth was 0.5 ps, tunable from 790–870 nm, and the estimated maximum carrier density was $5 \times 10^{15}$ cm$^{-3}$. The focused spot radius was typically 15–20 $\mu$m. The combination of lock-in techniques and aperturing of the transmitted beams ensures that we only detect the change in probe transmission induced by the pump. We used a camera-imaging system to check that the pump and probe spots were overlapping on the sample. In these conditions, the rise time of the detected nonlinear signal is directly related to the sweep-out time [61]–[63].

In Fig. 11 we show our results for the sweep-out times measured for samples I and II, together with our earlier p–i–n quantum well sample [32]. This earlier sample had 0.9 $\mu$m of GaAs–$Al_{0.31}Ga_{0.69}As$ quantum wells with a well thickness of 65 Å and $L_b$ = 57 Å, and therefore has barriers similar to those of sample III. The values for the escape time given are the 10–90% rise time of the differential eletroabsorption signal, as has been used previously [32], [63]. On comparing the results for the three samples, we can come to general conclusions about the field and barrier dependence of the escape times and compare them to our understanding based on (1)–(5).

1) All three samples show a general trend to a reduction in escape time as the voltage is increased. The minima at 5, 7, and 10 V for the three samples are well explained by resonant tunneling of electrons between the first and second sublevels of adjacent quantum wells. The arrows in Fig. 11(a) and (b) show the resonant voltage deduced from independent spectroscopic studies on these same samples [47], [64], and also from low temperature photocurrent $I$–$V$ characteristics (see Fig. 4). The coincidence of the resonant voltages measured by independent techniques and the minima in the escape time confirms our assignment of the escape time minima to electron resonant tunneling, and also indicates that space charge effects are negligible at the carrier densities gen-

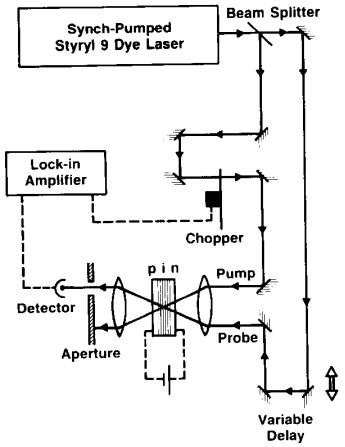


Fig. 10. Pump-probe apparatus used for the time-resolved differential electroabsorption measurements. The beam splitting ratio was adjsuted so that the ratio of pump : probe intensities was typically 10 : 1.

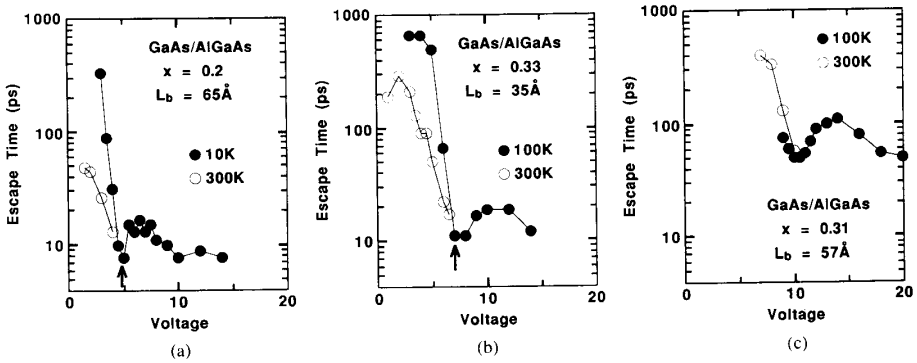


Fig. 11. Sweep-out time versus reverse bias for (a) sample I, (b) sample II, and (c) our previous quantum well sample. Results are shown for both room temperature and either 10 or 100 K. The arrows in (a) and (b) indicate the electron resonant tunneling voltage found from independent spectroscopic studies of these samples.

erated. At fields well above the resonance, the escape time limits out to a value of around 10 ps for samples I and II. This time corresponds to the average transit time of the carriers through the 1 $\mu$m intrinsic region at a saturation drift velocity of $\sim 10^7$ cms$^{-1}$, and represents an effective lower limit on the escape times that can be measured by this technique. The reduction of escape time with applied field can be caused by either an increase in the thermionic emission rate or the tunneling rate [see (3)–(5)]. These measurements are consistent with the measured increase in saturation intensity with voltage.

2) On comparing Fig. 11(a) and (c), we see that a reduction in $x$ at approximately constant $L_b$ leads to a reduction in the escape time. Again, this is consistent with either enhanced tunneling or thermionic emission, although the latter would seem more likely. These results confirm that the most likely cause of the increase in $I_s$ on reducing $x$ is the reduction in the sweep-out time.

3) On comparing Fig. 11(b) and (c) we see how a reduction in $L_b$ at approximately constant $x$ leads to a reduction in the carrier escape time. This is characteristic of a tunneling event, and cannot be explained in terms of pure thermionic emission. The result explains the increase in $I_s$ observed on reducing $L_b$, and also the faster SEED switching time measured for samples with 35 Å barriers compared to 60 Å [4].

4) The escape times of all three samples are very sensitive to temperature at low voltages, but practically independent of $T$ above resonant voltage. (The fact that we give no data points in Fig. 11(c) at 100 K below 9 V indicates a very long lifetime.) This result suggests that the escape process is thermally assisted at low fields, and proceeds by tunneling at high fields. A simple explanation of why this might be so has been given by Larsson *et al.* [17]. They argued that at low fields a pure tunneling escape mechanism is unlikely due to the large number of

barriers that must be crossed. On the other hand, at high fields the carriers need only tunnel through a single barrier, and therefore this process has a high probability. Since the low-field escape time is also affected by the barrier width [cf. point 3) above], the most likely explanation seems to involve a thermally-assisted tunneling escape mechanism.

In order to investigate the low-field thermally-assisted escape mechanism, we examined the temperature dependence of the escape time of sample I at 3.0 V in more detail. Fig. 12 shows the variation of the measured sweep-out time against temperature. We find two different types of behavior. Up to 100 K, the sweep-out time is independent of the temperature, while above 100 K it decreases rapidly with $T$. Around room temperature, the measured escape time begins to limit out at the sample transit time of $\sim 10$ ps. These results are consistent with the temperature-dependent satuation measurements shown in Fig. 9. The results can be readily explained on the basis of (1), (3), and (5). These equations show that at low temperatures, thermal emission is frozen out, and the escape time is determined by tunneling, which depends only very weakly on $T$. We thus deduce a value of 330 ps for the tunneling time. At sufficiently high temperatures, thermal emission must become the dominant escape mechanism, and we can use (1) to deduce $\tau_E$. To do this we subtracted the 13 ps sample transit time from the measured sweep-out time, and we assumed that $\tau_R$ is negligible. The simple allowance for the transit effects becomes less reliable for the data points at higher temperatures. The deduced values of $\tau_E$ are plotted on a logarithmic scale against $T^{-1}$ in the inset of Fig. 12 between 140 K and room temperature. This Arrenhius plot gives the activation energy as $49 \pm 15$ meV at 3.0 V. The $\pm 15$ meV uncertainty is based on the sensitivity of the fit to variations in the activation energy, and also on the estimated accuracy of the thermal emission times. The curve fitted to the sweep-out times in Fig. 12 was obtained from (1) with tunneling and transit times of 330 and 13 ps, respectively. The thermal emission time was taken from the straight line fit in the inset. We repeated this analysis at 3.5 V, and found a tunneling time of 100 ps and thermal activation energy of 47 meV.

In order to obtain a clearer understanding of the physical significance of the activation energy, we show in Fig. 13 a sketch of the electron and heavy hole energy levels of the sample at an applied field of 45 kV cm$^{-1}$, corresonding to about 3.0 V applied bias after allowing for the built-in voltage. The levels were found by fitting the low temperature optical absorption spectra using the tunneling resonance technique to find the subband energies at finite field. The $x$ value of the AlGaAs was determined to be 0.19 from the absorption edge of the top $Al_xGa_{1-x}As$ p-type contact, and also from X-ray measurements. We assumed a band offset ratio $Q_c : Q_v$ of 67:33 [65]. The shaded bands indicate the energies which correspond to the experimentally determined limits of the activation energy. We see that the activation energy seems to correspond to two possible escape mechanisms: either emission of heavy holes over the top of their confining barrier, or the onset of coupling of electrons to continuum states through just one barrier. Our other results show the sensitivity of the escape process to the barrier thickness at low fields, and so the latter mechanism seems more likely. The proposed escape mechanism via thermal occupation of higher subbands [17], [24] does not appear to be consistent with our data. Similarly, the simple emission of electrons over the top of their barrier is inconsistent with our results. There is, however, another escape mechanism which would account for the deduced activation energies, namely, phonon-assisted tunneling [31], [66]–[68]. Our measured activation energy is consistent with the energy of the AlAs-like $LO$-phonon mode in the AlGaAs barrier.

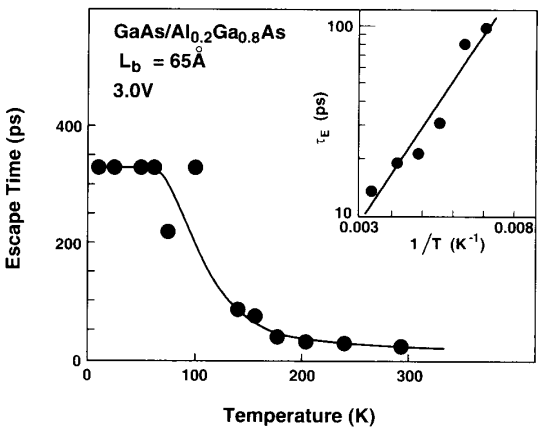


Fig. 12. Escape time for sample I between 10 K and room temperture at 3.0 V against temperature $T$. The inset shows an Arrhenius plot of the thermal emission time between 140 K and room temperature deduced from the escape time assuming a tunneling time of 330 ps and a transit time of 13 ps. The straight line fit is for an activation energy of 49 meV. The curve fitted to the escape time assumes the same fitting parameters as for the straight line fit in the inset.

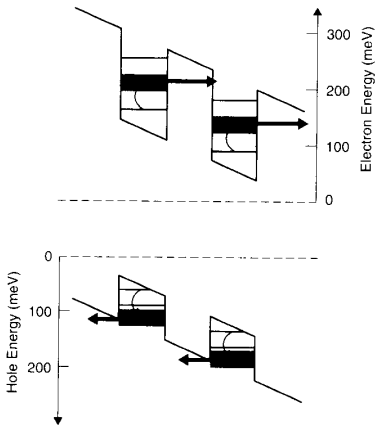


Fig. 13. Electron and heavy hole energy level diagram of sample I at 45 kV cm$^{-1}$ applied field, which corresponds to 3.0 V applied reverse bias. The shaded bands indicate the range of energies which might participate in the thermally-activated escape mechanism.

Further work will be needed to determine the escape mechanism more precisely.

A question remains as to whether the sweep-out times measured in this way are for electrons or holes, or a convolution of both. The experiment measures the fastest escaping carriers, which are usually presumed to be the electrons. From the discussion in Section II, we do not consider it justified to make such a presumption for the GaAs–AlGaAs system because of the possibility of very rapid hole thermal emission. However, the fact that we do see a minimum at the field for resonant tunneling of electrons does seem to suggest that the sweep-out times refer to electrons only.

## VII. Conclusions

We have demonstrated the importance of the carrier sweep-out physics both for the excition saturation intensity and for the electroabsorption. We have shown that the exciton saturation intensity can be increased by using low or thin barriers, without significant loss to the electroabsorption performance. This result is particularly important for SEED systems. We have also shown that the exciton saturation intensity increases with applied field. Our time-resolved measurements indicate that the sweep-out mechanism is thermally assisted at low fields. The precise mechanism is yet to be resolved, but is probably either thermal excitation of the electrons to the point where they can couple to continuum states through just a single barrier, or alternatively, optical phonon-assisted tunneling. At high fields, the escape mechanism is probably pure tunneling. The behavior of the holes is still not fully understood, and more work will be needed in this area before arriving at a quantitative analysis of the exciton saturation intensity. An improvement in the understanding of the sweep-out physics should lead to further advances such as the recently demonstrated 33 ps optical SEED switch [4].

## Acknowledgment

We are endebted to J. E. Henry and M. M. Becker for the processing of the samples. We would like to thank G. D. Boyd, K. Leo, T. Sizer, and D. S. Chemla for many helpful discussions.

## References

[1] D. A. B. Miller, D. S. Chemla, T. C. Damen, A. C. Gossard, W. Wiegmann, T. H. Wood, and C. A. Burrus, "Novel hybrid optically bistable switch: The quantum well electro-optic effect device," *Appl. Phys. Lett.*, vol. 45, pp. 13–15, 1984.

[2] For a recent review, see D. A. B. Miller, "Quantum-well self-electro-optic effect devices," *Opt. and Quantum Electron.*, vol. 22, pp. S61–S98, 1990.

[3] D. A. B. Miller, D. S. Chemla, T. C. Damen, A. C. Gossard, W. Wiegmann, T. H. Wood, and C. A. Burrus, "Electric field dependence of optical absorption near the band gap of quantum-well structures," *Phys. Rev. B.*, vol. 32, pp. 1043–1060, 1985.

[4] G. D. Boyd, A. M. Fox, D. A. B. Miller, L. M. F. Chirovsky, L. A. D'Asaro, J. M. Kuo, R. F. Kopf, and A. L. Lentine, "33 ps optical switching of symmetric self electro-optic effect device," *Appl. Phys. Lett.*, vol. 57, pp. 1843–1845, 1990.

[5] A. L. Lentine, L. M. F. Chirovsky, and L. A. D'Asaro, "Photonic ring counter using batch fabricated symmetric self electro-optic effect devices," *Opt. Lett.*, vol. 16, pp. 36–38, 1991.

[6] A. M. Fox, D. A. B. Miller, G. Livescu, J. E. Cunningham, J. E. Henry, and W. Y. Jan, "Exciton saturation in electrically biased quantum wells," *Appl. Phys. Lett.*, vol. 57, pp. 2315–2317, 1990.

[7] G. Lasher and F. Stern, "Spontaneous and stimulated recombination radiation in semiconductors," *Phys. Rev. A*, vol. 133, pp. 553–563, 1964.

[8] T. Matsusue and H. Sakaki, "Radiative recombination coefficient of free carriers in GaAs-AlGaAs quantum wells and its dependence on temperature," *Appl. Phys. Lett.*, vol. 50, pp. 1429–1431, 1987.

[9] E. E. Mendez, G. Bastard, L. L. Chang, L. Esaki, H. Morkoç, and R. Fischer, "Effect of electric field on the luminescence of GaAs quantum wells," *Phys. Rev. B*, vol. 26, pp. 7101–7104, 1982.

[10] H.-J. Polland, L. Shultheis, J. Kuhl, E. O. Göbel, and C. W. Tu, "Lifetime enhancement of two-dimensional excitons by the quantum-confined Stark effect," *Phys. Rev. Lett.*, vol. 55, pp. 2610–2613, 1985.

[11] M. G. Shorthose, A. C. Maciel, J. F. Ryan, M. D. Scott, A. Moseley, J. I. Davies and J. R. Riffat, "Electric field dependent exciton energy and photluminescence quenching in GaInAs/InP quantum wells," *Appl. Phys. Lett.*, vol. 51, pp. 493–495, 1987.

[12] H. Schneider and K. v. Klitzing, "Thermionic emission and Gaussian transport of holes in a GaAs/$Al_xGa_{1-x}As$ multiple-quantum-well structure," *Phys. Rev. B*, vol. 38, pp. 6160–6165, 1988.

[13] See, for example, B. A. Wilson, P. Dawson, C. W. Tu, and R. C. Miller, "Optical evidence of staggered band alignments in (Al, Ga)As/AlAs multi-quantum well structures," *J. Vac. Sci. Technol. B*, vol. 4, pp. 1037–1040, 1986.

[14] R. T. Collins, K. v. Klitzing, and K. Ploog, "Photoexcited transport in GaAs/AlAs quantum wells," *Appl. Phys. Lett.*, vol. 49, pp. 406–408, 1986.

[15] K. K. Choi, B. F. Levine, R. J. Malik, J. Walker, and C. G. Bethea, "Periodic netative conductance by sequential resonant tunneling through an expanding high-field superlattic domain," *Phys. Rev. B.*, vol. 35, pp. 4172–4175, 1987.

[16] M. Dutta, K. K. Choi, and P. G. Newman, "Thermionic emission and photoluminescence studies of the energy states of GaAs/AlAs superlattices," *Appl. Phys. Lett.*, vol. 55, pp. 2429–2431, 1989.

[17] A. Larsson, P. A. Andrekson, S. T. Eng, and A. Yariv, "Tunable superlattice p-i-n photodetectors: characteristics, theory, and applications," *IEEE J. Quantum Electron.*, vol. 24, pp. 787–801, 1988.

[18] T. B. Norris, X. L. Song, W. J. Schaff, L. F. Eastman, G. Wicks, and G. A. Mourou, "Tunneling escape time of electrons from a quantum well under the influence of an electric field," *Appl. Phys. Lett.*, vol. 54, pp. 60–62, 1989.

[19] F. Capasso, K. Mohammed, A. Y. Cho, R. Hull, and A. L. Hutchinson, "New quantum photoconductivity and large photocurrent gain by effective-mass filtering in a forward-biased superlattice p–n junction," *Phys. Rev. Lett.*, vol. 55, pp. 1152–1155, 1985; also "Effective mass filtering: Giant quantum amplification of the photocurrent in a semiconductor superlattice," *Appl. Phys. Lett.*, vol. 47, pp. 420–422, 1985.

[20] J. A. Kash, E. E. Mendez, and H. Morkoç, "Electric field induced decrease of photoluminescence lifetime in GaAs quantum wells," *Appl. Phys. Lett.*, vol. 46, pp. 173–175, 1985.

[21] E. J. Austin and M. Jaros, "Electric field induced shifts and lifetimes in GaAs-AlGaAs quantum wells," *Appl. Phys. Lett.*, vol. 47, pp. 274–276, 1985.

[22] Y. Horikoshi, A. Fischer, and K. Ploog, "Photoluminescence quenching in reverse-biased $Al_xGa_{1-x}As$/GaAs quantum-well heterostructures due to carrier tunneling," *Phys. Rev. B*, vol. 31, pp. 7859–7864, 1985.

[23] F. Y. Juang, J. Singh, P. K. Bhattacharya, K. Bajema, and R. Merlin, "Field-dependent linewidths and photoluminescence energies in GaAs-AlGaAs multiquantum well modulators," *Appl. Phys. Lett.*, vol. 48, pp. 1246–1248, 1986.

[24] H. Schneider, K. von Klitzing, and K. Ploog, "Resonant and nonresonant tunneling in GaAs/AlAs multi-quantum well structures," *Superlat. and Microstruct.*, vol. 5, pp. 383–396, 1989.

[25] S. Tarucha and K. Ploog, "Dependence of transient resonant-tunneling charactersitics on barrier thickness in AlAs/GaAs multiple-quantum-well structures," *Phys. Rev. B*, vol. 39, pp. 5353–5360, 1989.

[26] H. Schneider, W. W. Rühle, K. v. Klitzing, and K. Ploog, "Electrical and optical time-of-flight measurements in GaAs/AlAs superlattices," *Appl. Phys. Lett.*, vol. 54, pp. 2656–2658, 1989.

[27] M. Tsuchiya, T. Matsusue, and H. Sakaki, "Tunneling escape rate of electrons from quantum well in double-barrier heterostructures," *Phys. Rev. Lett.*, vol. 59, pp. 2356-2359, 1987.

[28] T. Tada, A. Yamaguchi, T. Ninomiya, H. Uchiki, T. Kobayashi, and T. Yao, "Tunneling process in AlAs/GaAs double quantum wells studied by photoluminescence," *J. Appl. Phys.*, vol. 63, pp. 5491-5494, 1988.

[29] M. K. Jackson, M. B. Johnson, D. H. Chow, T. C. McHill, and C. W. Nieh, "Electron tunneling time measured by photoluminescence excitation correlation spectroscopy," *Appl. Phys. Lett.*, vol. 54, pp. 552-554, 1989.

[30] R. J. Manning, P. J. Bradley, A. Miller, J. S. Roberts, P. Mistry, and M. Pate, "Electric-field-dependent photoresponse of multiple quantum well modulator," *Electron. Lett.*, vol. 25, pp. 269-270, 1989.

[31] M. G. Shorthose, J. F. Ryan, and A. Moseley, "Phonon-assisted tunneling of photoexcited carriers from InGaAs quantum wells in applied electric fields," *Solid State Electron.*, vol. 32, pp. 1449-1453, 1989.

[32] G. Livescu, A. M. Fox, D. A. B. Miller, T. Sizer, W. H. Knox, A. C. Gossard, and J. H. English, "Resonantly enhanced electron tunneling rates in quantum wells," *Phys. Rev. Lett.*, vol. 63, pp. 438-441, 1989.

[33] D. Y. Oberli, J. Shah, T. C. Damen, C. W. Tu, T. Y. Chang, D. A. B. Miller, J. E. Henry, R. F. Kopf, N. Sauer, and A. E. DiGiovanni, "Direct measurement of resonant and nonresonant tunneling times in asymmetric coupled quantum wells," *Phys. Rev. B*, vol. 40, pp. 3028-3031, 1989.

[34] H. Sakaki, T. Matsusue, and M. Tsuchiya, "Resonant tunneling in quantum heterostructures: electron transport, dynamics, and device applications," *IEEE J. Quantum Electron.*, vol. 25, pp. 2498-2504, 1989.

[35] M. Nido, M. G. W. Alexander, W. W. Rühle, T. Schweizer, and K. Köhler, "Nonresonant electron and hole tunneling times in $GaAs/Al_{0.35}Ga_{0.65}As$ asymmetric double quantum wells," *Appl. Phys. Lett.*, vol. 56, pp. 355-357, 1990.

[36] K. Leo, J. Shah, E. O. Göbel, T. C. Damen, K. Köhler, and P. Ganser, "Tunneling in semiconductor heterostructures studied by subpicosecond four-wave mixing," *Appl. Phys. Lett.*, vol. 56, pp. 2031-2033, 1990.

[37] K. Leo, J. Shah, J. P. Gordon, T. C. Damen, D. A. B. Miller, C. W. Tu, and J. E. Cunningham, "Effect of collisions and relaxation on coherent resonant tunneling: hole tunneling in $GaAs/Al_xGa_{1-x}As$ double-quantum well structures," *Phys. Rev. B*, vol. 42, pp. 7065-7068, 1990.

[38] K. Leo, J. Shah, E. O. Göbel, T. C. Damen, S. Schmitt-Rink, W. Schäfer, and K. Köhler, "Coherent oscillations of a wave packet in a semiconductor double-quantum-well structure," *Phys. Rev. Lett.*, vol. 66, pp. 201-204, 1991.

[39] I. Bar Joseph, G. Sucha, D. A. B. Miller, D. S. Chemla, B. I. Miller, and U. Koren, "Self-electro-optic-effect device and modulation convertor with InGaAs/InP multiple quantum wells," *Appl. Phys. Lett.*, vol. 52, pp. 51-53, 1988.

[40] R. Sauer, K. Thonke, and W. T. Tsang, "Photoinduced space-charge buildup by asymmetric electron and hole tunneling in coupled quantum wells," *Phys. Rev. Lett.*, vol. 61, pp. 609-612, 1988.

[41] R. E. Cavicchi, D. V. Lang, D. Gershoni, A. M. Sergent, H. Temkin, and M. B. Panish, "Sequential screening layers in photoexcited $In_xGa_{1-x}As/InP$ superlattice," *Phys. Rev. B*, vol. 38, pp. 13474-13477, 1988.

[42] T. H. Wood, J. Z. Pastalan, C. A. Burrus, Jr., B. C. Johnson, B. I. Miller, J. L. deMiguel, U. Koren, and M. G. Young, "Electric field screening by photogenerated holes in multiple quantum wells: a new mechanism for absorption saturation," *Appl. Phys. Lett.*, vol. 57, pp. 1081-1083, 1990.

[43] E. T. Tu, M. K. Jackson, and T. C. McGill, "Hole tunneling times in GaAs/AlAs double-barrier structures," *Appl. Phys. Lett.*, vol. 55, pp. 744-746, 1989.

[44] B. Deveaud, J. Shah, T. C. Damen, and W. T. Tsang, "Capture of electrons and holes in quantum wells," *Appl. Phys. Lett.*, vol. 52, pp. 1886-1888, 1988.

[45] D. S. Chemla, D. A. B. Miller, P. W. Smith, A. C. Gossard, and W. Wiegmann, "Room temperature excitonic nonlinear absorption and refraction in GaAs/AlGaAs multiple quantum well structures," *IEEE J. Quantum Electron*, vol. QE-20, pp. 265-275, 1984.

[46] W. H. Knox, R. L. Fork, M. C. Downer, D. A. B. Miller, D. S. Chemla, C. V. Shank, A. C. Gossard, and W. Wiegmann, "Femtosecond dynamics of resonantly excited excitons in room-temperature GaAs quantum wells," *Phys. Rev. Lett.*, vol. 54, pp. 1306-1309, 1985.

[47] A. M. Fox, D. A. B. Miller, G. Livescu, J. E. Cunningham, J. E. Henry, and W. Y. Jan, "Excitons in resonantly coupled quantum wells," *Quantum-Well and Superlattice Physics III*, G. H. Döhler, E. S. Koteles, J. N. Schulman, Eds. in *Proc. SPIE*, vol. 1283, pp. 164-174, 1990.

[48] R. A. Morgan, J. M. Freund, L. M. F. Chirovsky, L. A. D'Asaro, R. F. Kopf, and J. M. Kuo, "Improvements in self electro-optic effect devices using reduced-barrier multiple quantum wells," in *Conf. Dig.*, LEOS'90, paper OE8.2, p. 156.

[49] D. A. B. Miller, D. S. Chemla, D. J. Eilenberger, P. W. Smith, A. C. Gossard, and W. T. Tsang, "Large room-temperature optical nonlinearity in $GaAs/Ga_{1-x}Al_xAs$ multiple quantum well structures," *Appl. Phys. Lett.*, vol. 41, pp. 679-681, 1982.

[50] J. S. Weiner, D. B. Pearson, D. A. B. Miller, D. S. Chemla, D. Sivco, and A. Y. Cho, "Nonlinear spectroscopy of InGaAs/InAlAs multiple quantum well structures," *Appl. Phys. Lett.*, vol. 49, pp. 531-533, 1986.

[51] A. M. Fox, A. C. Maciel, M. G. Shorthose, J. F. Ryan, M. D. Scott, J. I. Davies, and J. R. Riffat, "Nonlinear excitonic optical absorption in GaInAs/InP quantum wells," *Appl. Phys. Lett.*, vol. 51, pp. 30-32, 1987.

[52] K. Tai, J. Hegarty, and W. T. Tsang, "Nonlinear spectroscopy in $In_{0.53}Ga_{0.47}As/InP$ multiple quantum wells," *Appl. Phys. Lett.*, vol. 51, pp. 86-88, 1987.

[53] S. H. Park, J. F. Morhange, A. D. Jeffrey, R. A. Morgan, A. Chavez-Pirson, H. M. Gibbs, S. W. Koch, N. Peyghambarian, M. Derstine, A. C. Gossard, J. H. English, and W. Wiegmann, "Measurements of room-temperature band-gap-resonant optical nonlinearities of GaAs/AlGaAs multiple quantum wells and bulk GaAs," *Appl. Phys. Lett.*, vol. 52, pp. 1201-1203, 1988.

[54] M. G. Shorthose, A. C. Maciel, J. R. Ryan, M. D. Scott, J. I. Davies, and A. Moseley, "Optical studies of excitons in GaInAs/InP quantum wells grown by low-pressure metal-organic vapour-phase epitaxy," *Semicond. Sci. Technol.*, vol. 3, pp. 616-619, 1988.

[55] A. Miller, R. J. Manning, P. K. Milsom, D. C. Hutchings, D. W. Crust, and K. Woodbridge, "Transient grating studies of excitonic optical nonlinearities in GaAs/AlGaAs multiple-quantum-well structures," *J. Opt. Soc. Amer. B*, vol. 6, pp. 567-578, 1989.

[56] M. Wegener, I. Bar Joseph, G. Sucha, M. N. Islam, N. Sauer, T. Y. Chang, and D. S. Chemla, "Femtosecond dynamics of excitonic absorption in the infrared $In_xGa_{1-x}As$ quantum wells," *Phys. Rev. B*, vol. 39, pp. 12794-12801, 1989.

[57] S. Schmitt-Rink, D. S. Chemla, and D. A. B. Miller, "Theory of transient optical nonlinearities in semiconductor quantum-well structures," *Phys. Rev. B*, vol. 32, pp. 6601-6609, 1985.

[58] ——, "Linear and nonlinear optical properties of semiconductor quantum wells," *Adv. Phys.*, vol. 38, pp. 89-188, 1989.

[59] S. Hong and J. Singh, "Study of excitons in an arbitrarily shaped $GaAs/Al_{0.3}Ga_{0.7}As$ single quantum well in the presence of static transverse electric field," *J. Appl. Phys.*, vol. 61, pp. 5346-5352, 1987.

[60] S. Nojima, "Electric field dependence of the exciton binding energy in $GaAs/Al_xGa_{1-x}As$ quantum wells," *Phys. Rev. B*, vol. 37, pp. 9087-9088, 1988.

[61] R. J. Manning, P. J. Bradley, A. Miller, J. S. Roberts, P. Mistry, and M. Pate, "Photoconductive response time of a multiple quantum well *pin* modulator," *Electron. Lett.*, vol. 24, pp. 854-855, 1988.

[62] G. Livescu, D. A. B. Miller, T. Sizer, D. J. Burrows, J. E. Cunningham, A. C. Gossard, and J. H. English, "High-speed absorption recovery in quantum well diodes by diffusive electrical conduction," *Appl. Phys. Lett.*, vol. 54, pp. 748-750, 1989.

[63] G. Livescu, A. M. Fox, D. A. B. Miller, T. Sizer, W. H. Knox, J. E. Cunningham, A. C. Gossard, and J. H. English, "Optical detection of resonant tunneling of electrons in quantum wells," *Semicond. Sci. and Technol.*, vol. 5, pp. 549-556, 1990.

[64] A. M. Fox, D. A. B. Miller, G. Livescu, J. E. Cunningham, J. E. Henry, and W. Y. Jan, "Excitons in resonant coupling of quantum wells," *Phys. Rev. B*, vol. 42, pp. 1841-1844, 1990.

[65] K. J. Moore, P. Dawson, and C. T. Foxon, "Effects of electronic coupling on the band alignment of thin GaAs/AlAs quantum-well structures," *Phys. Rev. B*, vol. 38, pp. 3368-3374, 1988.

[66] V. J. Goldman, D. C. Tsui, and J. E. Cunningham, "Evidence of LO-phonon-emission-assisted tunneling in double-barrier heterostructures," *Phys. Rev. B*, vol. 36, pp. 7635-7637, 1987.

[67] M. L. Leadbeater, E. S. Alves, L. Eaves, M. Henini, O. H. Hughes, A. Celeste, J. C. Portal, G. Hill, and M. A. Pate, "Magnetic field studies of elastic scattering and optic-phonon emission in resonant tunneling devices," *Phys. Rev. B*, vol. 39, pp. 3438–3441, 1989.
[68] D. Y. Oberli, J. Shah, T. C. Damen, J. M. Kuo, J. E. Henry, J. Lary, and S. M. Goodnick, "Optical phonon-assisted tunneling in double quantum well structures," *Appl. Phys. Lett*, vol. 56, pp. 1239–1241, 1990.

**A. Mark Fox** was born in Lincolnshire, England, in 1961. He received the B.A. degree in physics from Oxford University in 1982 and the D.Phil degree in 1987. Between 1986 and 1988 he was a Junior Research Fellow in solid state physics at Christ Church College, Oxford.

In 1988 he joined the Department of Photonic Switching Device Research at AT&T Bell Laboratories, Holmdel, NJ, as a post-doctoral member of the Technical Staff. His research interests include nonlinear optics, ultrafast phenomena in solids, and the physics of low-dimensional semiconductor structures. In 1990 he returned to the Department of Physics, Oxford University, as a Royal Society University Research Fellow.

Dr. Fox is a member of the Optical Society of America and the Institute of Physics.

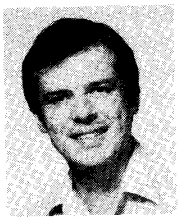

**David A. B. Miller** (M'84-SM'89) was born in Hamilton, U.K. He received the B.Sc. degree in physics from St. Andrews University, and performed his graduate studies at Heriot-Watt University, where he was a Carnegie Research Scholar, receiving the Ph.D. degree in 1979.

He continued to work at Heriot-Watt University, and later became a Lecturer with the Department of Physics. He moved to AT&T Bell Laboratories, Holmdel, NJ, in 1981 as a member of the Technical Staff, and since 1987 has been the Head of the Department of Photonics Switching Device Research. His research interests include nonlinear optics in semiconductors, optical switching, and the physics of quantum-confined structures. He has published over 140 technical papers, 4 book chapters, and holds 23 patents.

Dr. Miller is a Fellow of the Optical Society of America and the American Physical Society, and is a member of IEEE LEOS. During 1986–1987, he was a LEOS Traveling Lecturer. He was awarded the 1986 Adolph Lomb Medal for his contributions to semiconductor nonlinear optics, and was corecipient of the 1988 R. W. Wood Medal for his work on quantum-well optical properties.

**Gabriela Livescu** was born in Timisoara, Romania. She received the B.S. degree in physics from the University of Bucharest, Romania, in 1974 and the Ph.D. degree in physics from the Technion, Israel, in 1984.

She was a Research Associate at the City College of New York, before joining AT&T Bell Laboratories, Holmdel, NJ, in 1986, first as a post-doctoral member of the Technical Staff in the Department of Photonics Switching Research, until 1988 and then as a member of the Technical Staff in the Department of Optoelectronics Devices, Breinigsville, PA. She has been engaged in experimental research on optical properties of bulk semiconductors as well as quantum confined structures and devices. She extensively used a variety of techniques such as Raman scattering, photoluminescence, and steady-state and picosecond time-resolved optical absorption and electro-absorption.

Dr. Livescu is a member of the American Physical Society and the Optical Society of America.

**J. E. Cunningham** was born in Oak Ridge, TN, on November 30, 1949. He received the B.S. degree from the University of Tennessee in 1972 and the Ph.D. degree in 1979 from the University of Illinois.

He remained at the University of Illinois as a Senior Research Physicist and worked on molecular beam epitaxy of metallic superlattices as well as the optical properties of surfaces. Since joining AT&T Bell Laboratories, Holmdel, NJ, as a member of the Technical Staff in 1985, he has investigated compound semiconductor growth using gaseous sources.

Dr. Cunningham is a member of the American Physical Society.

**William Y. Jan** received the B.A. degree in physics from Rutgers College, Rutgers University, New Brunswick, NJ, and the M.S. degree in material science from Stevens Institute of Technology, Hoboken, NJ, in 1985 and 1989, respectively.

He has been a member of the Technical Staff at AT&T Bell Laboratories, Holmdel, NJ, since 1985. From 1985 to 1987 he worked on the design and fabrication of high speed semiconductor lasers and photodetectors. Since 1987 he has been involved in semiconductor materials characterization and growth by GSMBE.